

Review

A Review of Effects of Femtosecond Laser Parameters on Metal Surface Properties

Hongfei Sun, Jiuxiao Li *, Mingliang Liu, Dongye Yang * and Fangjie Li 

School of Materials Engineering, Shanghai University of Engineering Science, Shanghai 201620, China

* Correspondence: ljiuxiao@126.com (J.L.); dongye.yang@sues.edu.cn (D.Y.)

Abstract: As a laser technology, the femtosecond laser is used in biomedical fields due to its excellent performance—its ultrashort pulses, high instantaneous power, and high precision. As a surface treatment process, the femtosecond laser can prepare different shapes on metal surfaces to enhance the material's properties, such as its wear resistance, wetting, biocompatibility, etc. Laser-induced periodic surface structures (LIPSSs) are a common phenomenon that can be observed on almost any material after irradiation by a linearly polarized laser. In this paper, the current research state of LIPSSs in the field of biomedicine is reviewed. The influence of laser parameters (such as laser energy, pulse number, polarization state, and pulse duration) on the generation of LIPSSs is discussed. In this paper, the applications of LIPSSs by femtosecond laser modification for various purposes, such as in functional surfaces, the control of surface wettability, the surface colonization of cells, and the improvement of tribological properties of surfaces, are reviewed.

Keywords: laser-induced periodic surface structures; femtosecond laser processing; functional surfaces; application



Citation: Sun, H.; Li, J.; Liu, M.; Yang, D.; Li, F. A Review of Effects of Femtosecond Laser Parameters on Metal Surface Properties. *Coatings* **2022**, *12*, 1596. <https://doi.org/10.3390/coatings12101596>

Academic Editors: Angela De Bonis and Anton Ficai

Received: 31 July 2022

Accepted: 22 September 2022

Published: 21 October 2022

Publisher's Note: MDPI stays neutral with regard to jurisdictional claims in published maps and institutional affiliations.



Copyright: © 2022 by the authors. Licensee MDPI, Basel, Switzerland. This article is an open access article distributed under the terms and conditions of the Creative Commons Attribution (CC BY) license (<https://creativecommons.org/licenses/by/4.0/>).

1. Introduction

In 1954, Charles Towns et al. [1] made the first maser, the precursor of the laser. It opened the door to a series of astonishing inventions and discoveries. D. E. Spence et al. [2] obtained the first laser with titanium-doped sapphire as the gain medium in 1991, which is considered to be the first femtosecond laser of real significance. Femtosecond lasers are used in various fields, such as information, environment, medicine, defense, and industry, because of their short pulses, high energy, and high peak power [3–13].

The femtosecond laser (fs-laser) has good application prospects in the biomedical field. There are various ways to improve the biocompatibility of medical implants, such as changing the alloy composition [14], designing porous structures [15], and various processes [16,17]. As a surface treatment process, the femtosecond laser can prepare different shapes on metal surfaces to enhance the material's properties, such as wear resistance, wetting, and biocompatibility [18–20]. Surface modification technologies include mechanical methods (e.g., friction stirring [21,22], burnishing [23]), chemical methods (e.g., anodic oxidation [24], chemical vapor deposition [25]) and physical methods (e.g., thermal spraying [26], physical vapor deposition [27]). Compared with traditional surface modification technology, laser surface modification has outstanding advantages, such as high precision, flexibility, versatility, etc.

In this paper, the application of femtosecond laser surface modification is reviewed in various fields and for various purposes, including in patterns, the coloration of functional surfaces, the control of surface wettability, the surface colonization of cells, and the improvement of tribological properties of nanostructured metal surfaces, and we explore the connection between femtosecond laser parameters and patterns to provide a reference for future applications.

2. Laser-Induced Periodic Stripe Structure (LIPSS) with Femtosecond Laser

A laser-induced periodic surface structure (LIPSS) is a surface relief composed of periodic lines that can be observed on almost any material after irradiation of a linearly polarized laser beam, especially when using ultrashort laser pulses of durations in the range of picoseconds to femtoseconds [28–36].

A lot of work has been performed to study the formation mechanism of the femtosecond laser on LIPSSs. A LIPSS can be classified according to the characteristic ratio of its spatial periods (Λ) to the irradiation wavelength (λ) and the polarization direction of the linear laser beam used to produce them [37–39]. Figure 1a provides a general classification of LIPSSs observed on irradiation with femtosecond laser pulses. The period of low spatial frequency LIPSSs (LSFL) is slightly equal to or less than the laser wavelength. They are perpendicular (LSFL-I) or parallel (LSFL-II) to the polarization direction of the laser. In contrast, the period of high spatial frequency LIPSSs (HSFL) is smaller than half of the irradiation wavelength and may be formed as deep surface gratings (HSFL-I, depth-to-period aspect ratio $A > 1$) or as shallow surface gratings (HSFL-II, depth-to-period aspect ratio $A < 1$). Figure 1b [37] provides an LSFL-I type structure on a Ti6Al4V surface after femtosecond laser irradiation. The double arrows indicate the direction of the laser beam polarization. The LSFL structure has a period of $\Lambda_{\text{LSFL}} \sim 620 \pm 80$ nm and is perpendicular to the polarization direction of the laser beam. Figure 1c shows the HSFL-II structure formed on the laser irradiation surface [40]. The HSFL structures have periods of less than 100 nm ($\Lambda_{\text{HSFL}} \sim 80 \pm 20$ nm) and are parallel to the direction of the laser beam polarization.

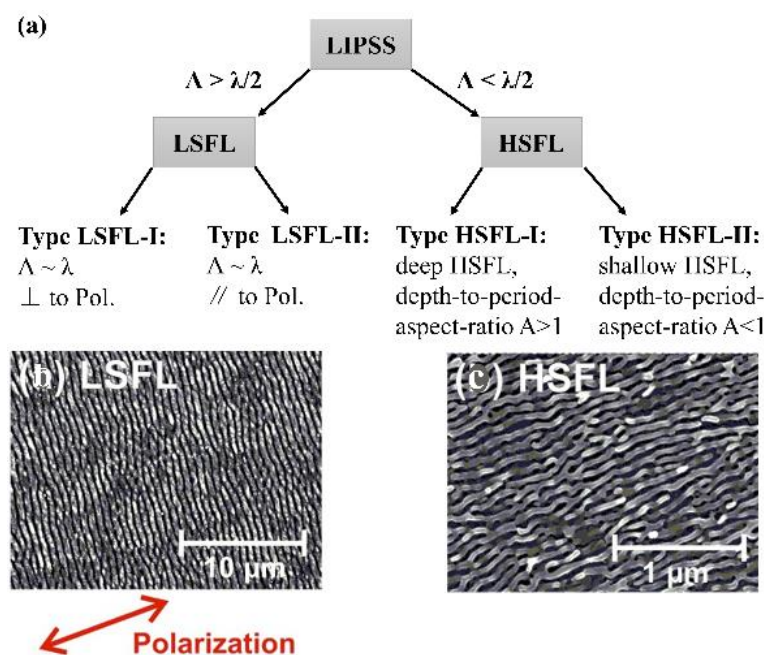
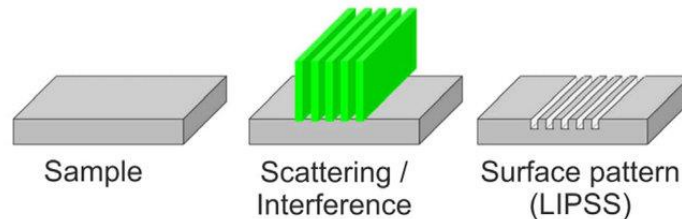


Figure 1. (a) General classification of fs-laser-induced periodic surface structures. SEM micrographs [37] of near wavelength LSFL-I (b) and sub-wavelength HSFL-II (c) on Ti6Al4V surfaces after irradiation with fs-laser in the air (pulse duration $\tau = 30$ fs, center wavelength $\lambda = 790$ nm, pulse repetition frequency 1 kHz). The double arrows in (b) mark the direction of laser beam polarization.

The current theories on the formation of LIPSSs can be divided into two classes, i.e.: (i) Electromagnetic theories describing the deposition of optical energy into a solid. By introducing the η of efficacy factors, the researchers analyzed the interaction of electromagnetic radiation with microscopic rough surfaces through theoretical and experimental combinations [41]. (ii) Matter reorganization theory, which is based on the redistribution of the surface matter (Figure 2 [38,42]). The researchers believe that HSFL is formed through the self-organization of irradiated materials and is related to the surface instability caused by atomic diffusion and surface erosion effects [43–46]. The difference between both classes

can be summarized as follows: electromagnetic scattering and absorption effects show the spatial signature of the structure during laser irradiation, and the reorganization of matter takes longer. Figure 2a shows that static thermal melting or ablation from a sample occurs on shorter time scales. The laser beam is marked in green. Figure 2b shows a dynamic response via self-organization from a laser-produced instability.

(a) Electromagnetic models



(b) Matter reorganization models

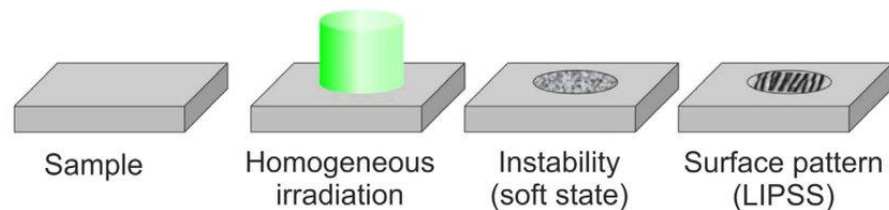


Figure 2. Ref. [42] Fundamental processes occur during LIPSS formation according to (a) electromagnetic models and (b) matter reorganization models. The laser irradiation is marked in green.

3. Laser Parameters That Control LIPSS

Studies have shown that laser peak fluence, the number of laser pulses, laser polarization state, pulse duration, and the processing environment are all key parameters affecting LIPSS [47–52].

3.1. Laser Fluence

The laser fluence has a large impact on the morphology of LIPSSs; different types of LIPSS are obtained by varying the laser fluence on the same material [49–51,53,54]. J. Bonse [55] obtained both LSFL and HSFL on the surface of titanium by varying the laser fluence, and the laser fluence affects the periodicity of LIPSSs. Georg Schnell et al. [50] report the formation of nano- and micro-structures on Ti6Al4V evoked by different scanning strategies and fluences with an fs-laser. Figure 3 shows the SEM microstructure images of the femtosecond laser pulses of different energy fluences. As shown in Figure 3a [50], the surface morphology is LIPSS when the laser fluence is 0.14 J/cm^2 , the surface topography is micron spacing grooves when the laser fluence is 0.86 J/cm^2 , and the surface morphology is cones and micro craters at a laser fluence of 4.76 J/cm^2 . Shi-zhen Xu et al. [56] explore the influence of laser scan fluence on the formation of micro/nanostructures on the surfaces of fused silica. At a fixed laser scan speed (1.7 mm/s), the HFSL was observed at a low fluence region ($1.8\text{--}2.5 \text{ J/cm}^2$). A transition from HSFL to LSFL occurred when a critical energy fluence threshold (2.5 J/cm^2) was exceeded (Figure 3b). The phenomenon can help to form process design guidelines to tailor large-scale surfaces with self-organized features, and can be used in future studies. For most materials, the periodicity of LIPSSs increases as the laser fluence increases. Better surface topography can be obtained at a low laser fluence approximate to the material ablation threshold. To achieve high efficiency for industrial applications, the ablation rate is increased by increasing the laser fluence. However, the processing quality is significantly reduced due to the thermal damage caused by the highly effective penetration depth. To avoid adverse effects on the sample, a suitable fluence is an advantageous condition to realize cold processing.

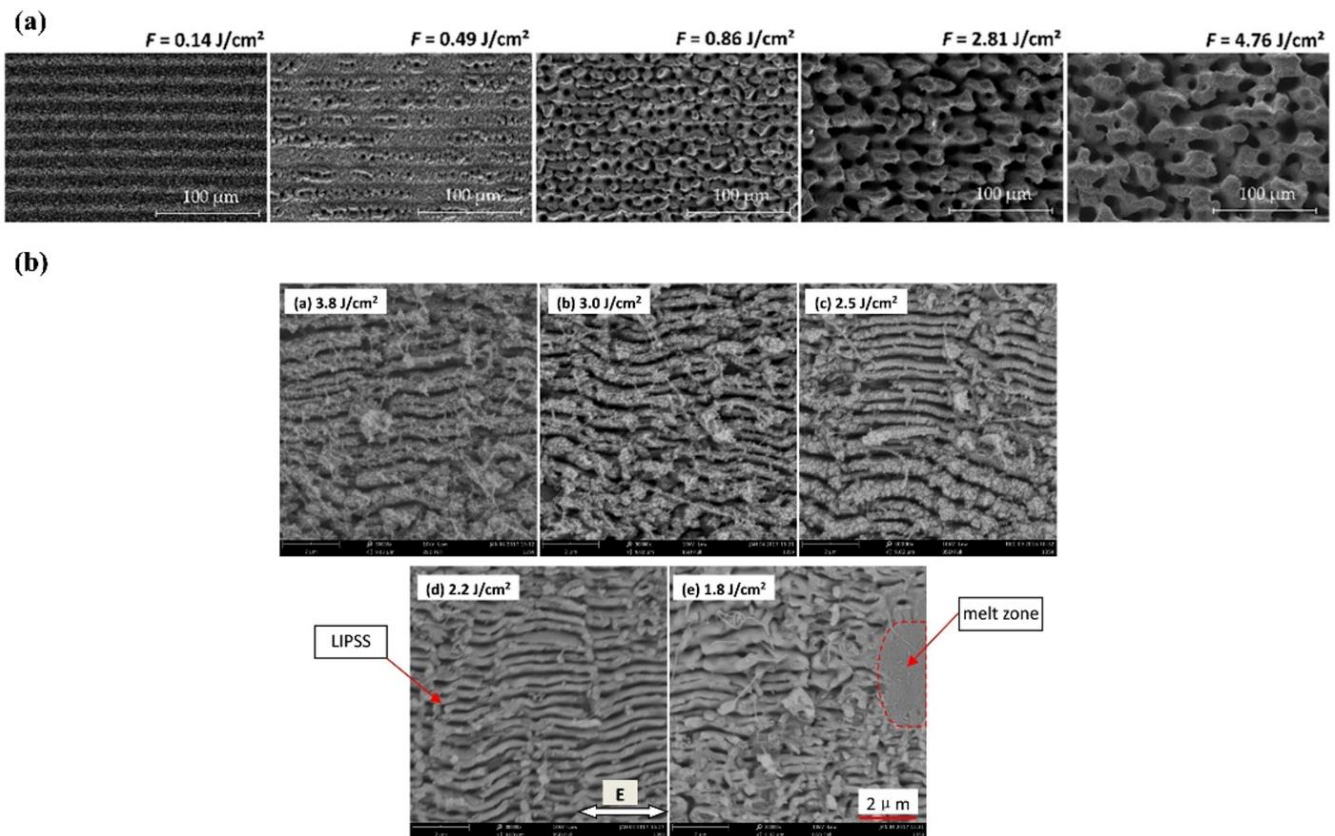


Figure 3. (a) Ref. [50] SEM images of structured surfaces with increasing laser fluence. (b) Ref. [56] Microstructures of femtosecond laser irradiation regions with different fluence.

3.2. Number of Pulses

The higher the number of laser pulses, the easier it is to obtain a more regular LIPSS. Evangelos Skoulas et al. [57] studied the effect of pulse number on the formation of LIPSSs. As the number of pulses increases, the surface roughness increases, and the period of LIPSS decreases. At the same time, as the number of pulses or the laser fluence increases, the depth of the pit and the height of the microstructure increase. Xu Ji et al. [58] prepared nanoholes on the silicon surface by a femtosecond laser. Figure 4 provides the SEM images of the depth of the surface pit and the height of the microstructure with the different numbers of pulses. As shown in Figure 4a, a shallow modified zone is formed with pulses. As shown in Figure 4b, when N is 4, the rectangular nanoholes were created on the silicon surface. As the number of pulses increases, the energy is absorbed more efficiently along the direction of laser polarization. This results in two rows of nanohole chains, forming LSFL, as shown in Figure 4c. For the pulse number, $N = 8$, the nanoholes become larger and deeper, as shown in Figure 4d. The deeper and larger nanoholes can be created on the surface by increasing the pulse number and fluences. When the pulse number increases to 10, most of the HSFL is broken, as shown in Figure 4e. Rao Li et al. [59] obtained the femtosecond laser-induced damage threshold (LIDT) by measuring the damage morphology under different energies and pulse numbers of the femtosecond laser. For the multi-pulse radiation, the LIDT of the thin film decreases as the number of pulses increases due to the accumulation effect. To obtain a high-quality periodic structure, it is necessary to accurately measure the laser damage threshold of the material.

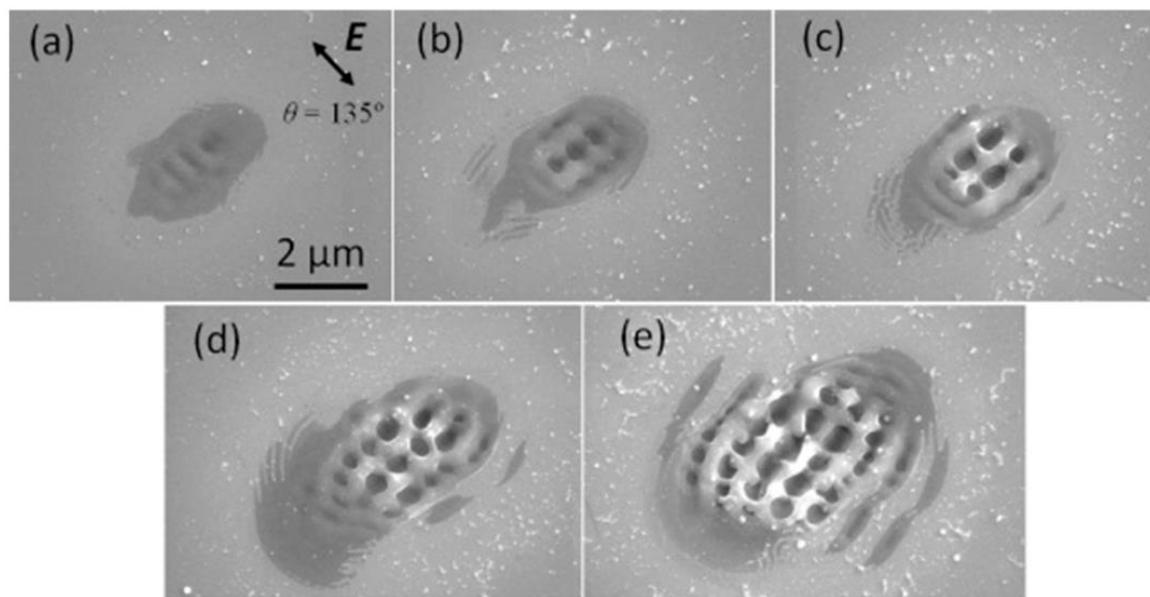


Figure 4. Ref. [58] SEM images of periodic structures induced on the surface of a silicon wafer by femtosecond laser at a fixed laser fluence ($F = 0.22 \text{ J/cm}^2$) with different pulse number (N): (a) $N = 2$, (b) $N = 4$, (c) $N = 6$, (d) $N = 8$ and (e) $N = 10$, respectively. The arrow shows the direction of laser polarization.

3.3. Polarization States

The structure characteristics of the material surface after femtosecond laser modification are related to the polarization state of the laser beam [60,61]. The orientation and shape of the laser-induced periodic structure are determined by the polarization of the incident light. For example, circularly polarized beams can acquire triangular periodic structures [62–64], and elliptically polarized beams can acquire spherical nanoparticles [65–67]. When a linearly polarized laser beam is applied, the ripple direction is perpendicular or parallel to the polarization direction of the incident laser beam. Zhang Hao et al. [48] used the finite-difference time-domain method (FDTD) to study the surface morphology of LIPSSs under various polarization states (linear, circular, radial and azimuthal). The surface morphology simulated using circular polarization lasers is consistent with the triangular LIPSSs and spherical nanoparticles reported in the literature [62,68]. Evangelos Skoulas et al. [57] obtained a nanoscale controllable periodic structure on the nickel surface by laser direct writing with radial and azimuthal polarization beams, which mimicked the placoid structures found in the skin of sharks. Figure 5 shows the characteristic surface morphologies attained in SEM micrographs obtained at a scanning speed $v = 0.5 \text{ mm/s}$ and a laser fluence $F = 0.24 \text{ J/cm}^2$, for linear Gaussian (a,b), radial (c,d) and azimuthal (e,f) cylindrical vector beams, respectively. The images (b,d,f) are higher magnifications of areas of the red dashed squares. As shown in Figure 5a, linear laser direct writing obtains LIPSSs on the surface. Figure 5b shows how the radial and azimuthal beams were irradiated to obtain a rhombus-like structure.

3.4. Pulse Duration

Pulse duration is a relevant parameter in laser processing, and different laser systems (e.g., nanosecond, picosecond, femtosecond) obtain different surface morphologies. Sun Yuanyuan et al. [69] used a continuous laser, nanosecond laser, and femtosecond laser to modify the surface of a ferromanganese alloy. The results show that the effect of the continuous laser and nanosecond laser on the material is mainly melted generation. Surface grooves in the micron range can be obtained using nanosecond lasers. Femtosecond laser ablation generates LIPSSs on the surface of the material without altering the crystal structure. LSFL can be obtained under laser irradiation with a nanosecond pulse duration or longer, while HSFL with periods much smaller than λ is only suitable for

the irradiation of ultrashort pulsed lasers in the range of picoseconds to femtoseconds. Sungkwon Shin et al. [70] ablated the Invar sheets with a laser with different pulse durations, and the results show that the femtosecond laser treatment obtained high precision micro-holes with no thermal damage (i.e., Figure 6). Figure 6a–c shows SEM images of laser pulses irradiating Invar, corresponding to the pulse durations of 10 ns, 15 ps, and 300 fs, respectively. In the ns laser processing with a laser fluence of 5 J/cm^2 , a pulse repetition rate of 50 Hz, and a wavelength of 248 nm, the surface is observed to produce burrs. High-precision micro-holes with no thermal damage at the edges were obtained by fs laser processing with $F = 0.29 \text{ J/cm}^2$, $f = 200 \text{ kHz}$, and $\lambda = 1035 \text{ nm}$.

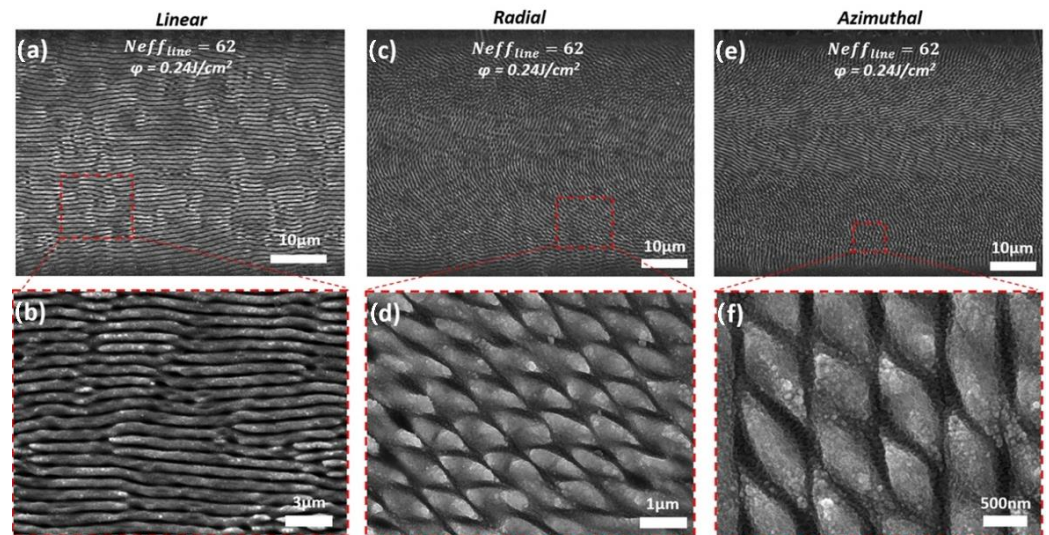


Figure 5. Ref. [57] The SEM images depicting line scans produced by linearly (a,b), radially (c,d), and azimuthally polarized (e,f) beams, respectively, at $v = 0.5 \text{ mm/s}$, and $F = 0.24 \text{ J/cm}^2$. The images (b,d,f) are higher magnifications of an area inside the red dashed squares and reveal the biomimetic shark skin-like morphology of the processed areas.

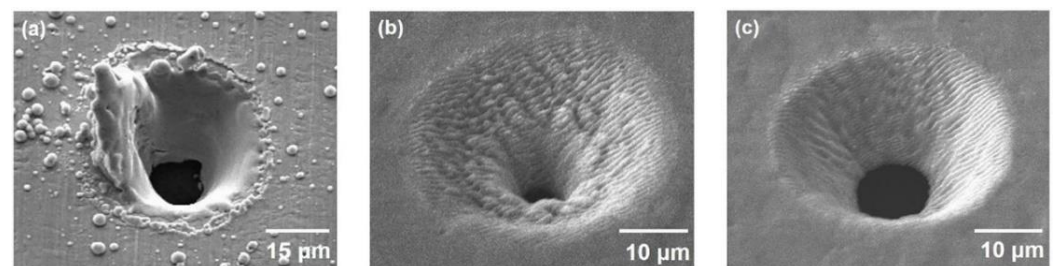


Figure 6. Ref. [70] SEM images of micro-holes on Invar were processed at three pulse durations of (a) 10 ns, (b) 15 ps, and (c) 300 fs, respectively. The ns laser parameters are $F = 5 \text{ J/cm}^2$, $f = 50 \text{ Hz}$, and $\lambda = 248 \text{ nm}$. For the ps and fs laser, $F = 0.29 \text{ J/cm}^2$, $f = 200 \text{ kHz}$, and $\lambda = 1035 \text{ nm}$.

3.5. Ambient Medium

In addition to the above laser-related parameters, the ambient medium around the sample also has a significant impact on the surface morphology of laser processing. Zhiduo Xin et al. [71] reported the results of femtosecond laser texturing and femtosecond laser nitriding experiments on Ti6Al4V. After femtosecond laser texturing, as shown in Figure 7a,c, cuboid structures of $125 \times 125 \times 130 \text{ nm}^3$ were formed on the surface. After nitriding, as shown in Figure 7b,d, a uniform crack-free TiN coating was prepared on the top of the textured structures with a thickness of 40–60 nm. As shown in Figure 7e, the morphology analysis shows that only slight height variations are introduced into the textured structures by femtosecond laser nitriding. Vadim Yalishev et al. [72] reported the surface morphology changes and wettability of titanium processed by femtosecond lasers in both the air and a

vacuum. The results show that the laser texture obtained under vacuum conditions can form a permanent superhydrophilic surface. Yang Yang et al. [73] studied the microstructure of the titanium action of femtosecond lasers in three different liquid environments. Cavities and islands were observed on the sample surface. After femtosecond laser modification in the supersaturated Hydroxyapatite (HA, $\text{Ca}_{10}(\text{PO}_4)_6(\text{OH})_2$) suspension, the biocompatible element Ca-P is firmly deposited on the surface. Thus, the corresponding functional surface can be obtained by changing the ambient medium, which also provides a new way to understand the ablation mechanism of the femtosecond laser.

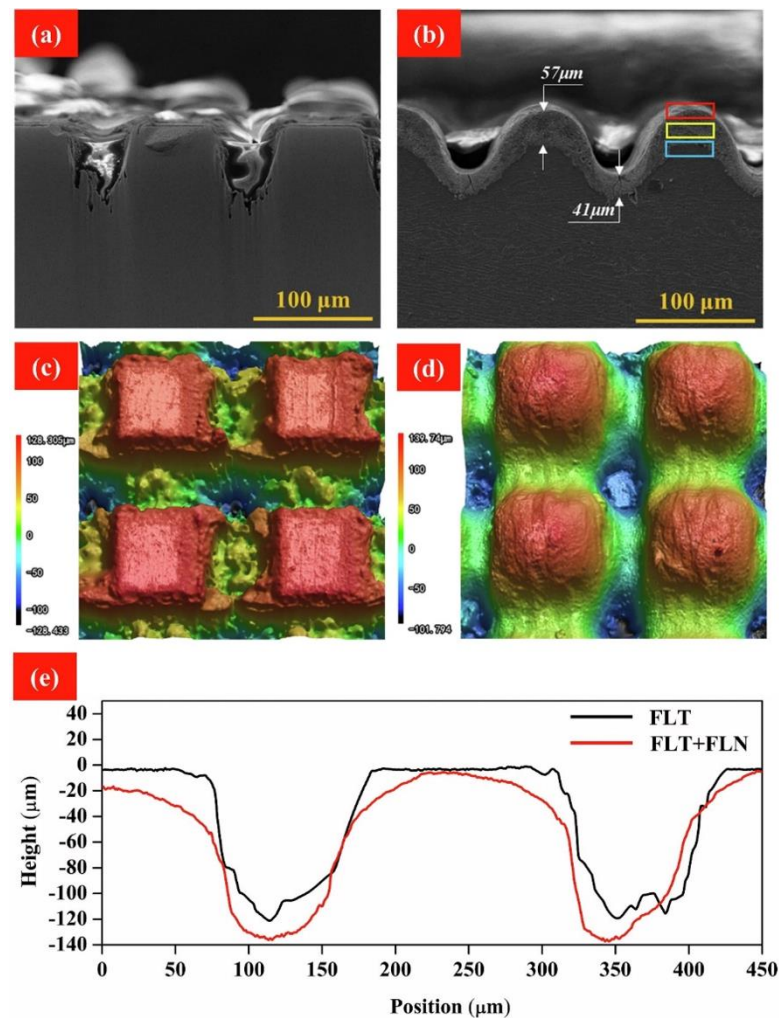


Figure 7. Ref. [71] The surface morphology and cross-section microstructure of the samples processed by Femtosecond laser texturing (FLT) and FLT+Femtosecond laser nitriding (FLN); (a) SEM image of FLT, (b) SEM image of FLT+FLN, (c) 3D morphology of the cross-section of FLT, (d) 3D morphology of the cross-section of FLT+FLN, (e) Profile curves corresponding to (c,d).

In summary, LIPSSs (ripples) can be obtained when the fluence of the laser is slightly greater than the ablation threshold of the material. Increasing the laser energy will obtain the surface morphology of grooves, pits, etc. In addition, the orientation and shape of LIPSSs are affected by the polarization state of the laser. An increase in the number of pulses will make the surface pits deeper. The laser processing environment is also one of the important parameters that affects surface morphology. Although the relevant parameters that affect the formation of LIPSSs have been reported, there is still a lack of a general algorithm to control the regularity of LIPSSs. In the future, artificial intelligence (AI) and algorithms will discover and control the regularity of LIPSSs.

4. Application of LIPSS

Surface texturing by laser irradiation can change various materials' properties and create multifunctional surfaces [74–78]. Materials can be better applied by customizing functional surfaces.

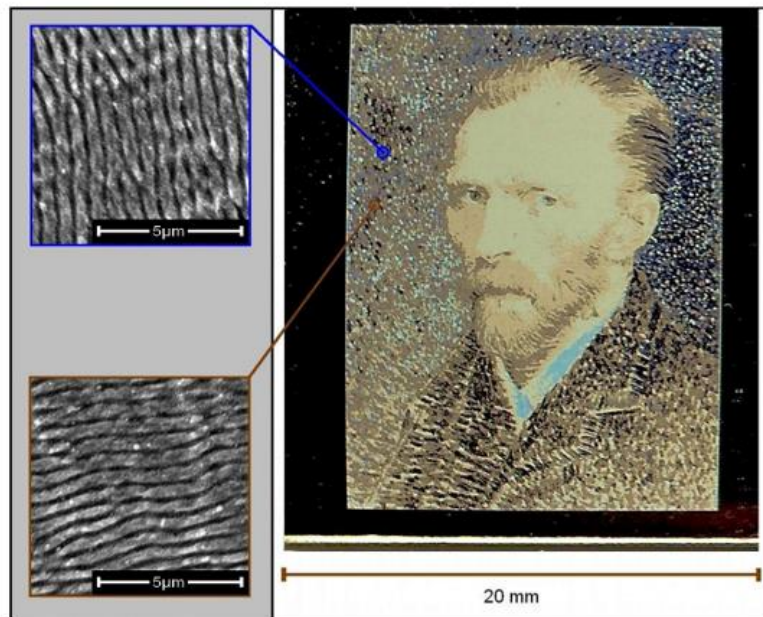
4.1. Structural Color

One of the most obvious applications of LIPSSs is optics. Since their period is in the same range as the radiation wavelength of visible light, they can effectively act as a diffraction grating, producing a “structural color”. B. Dusser et al. [79] studied how to change the direction of the ripples to transmit information onto metal surfaces, creating a portrait of Vincent van Gogh on stainless steel surfaces (Figure 8A). Wang Chao et al. [80] prepared LIPSSs on a Ti6Al4V surface by laser irradiation, and observed differences in the laser texture color under natural light, and the surface color changes with the changes in the laser parameters (Figure 8B). Figure 8B(a) shows an optical image of the sample after laser irradiation, which includes “nine-squares” and “JLU”. Figure 8B(b) lists the laser parameters corresponding to each square. As shown in Figure 8B(c), when captured in a dark environment, the difference in colors in the “nine squares” is evident. Moreover, as shown in Figure 8B(d), when changing the shooting angle, the “JLU” could present various colors. The results in Figure 8 show that the LIPSS has potential applications for Ti6Al4V surface coloring. Different colors can be observed by changing the laser parameters to regulate the period and direction of the LIPSS, as well as the incident light and the viewing angle [81–85]. High-quality and regular LIPSSs are prepared in large areas on metal surfaces, making it possible to apply them to optical sensors, anti-counterfeiting, decoration, and laser marking, etc.

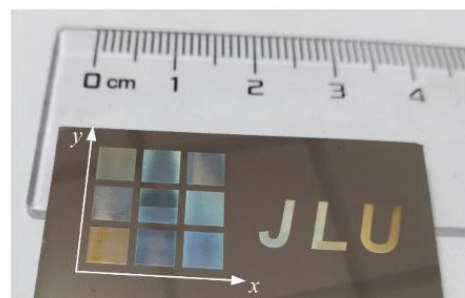
4.2. Wetting Behavior

The wetting behavior of LIPSSs has attracted the attention of many researchers. In general, the wettability of liquids to solid surfaces depends on three major factors: (1) the surface energy of the solids and liquids, (2) the viscosity of the liquids, and (3) the surface morphology of the solids. Surface topography can significantly affect the contact angle of droplets placed on the surface. Figure 9 shows that the surface morphology has a great effect on surface roughness and contact angle. The variation in the contact angles (θ_M) measured for 15 samples irradiated at different laser fluences is presented in Figure 9a. As the laser fluence increases, the contact angle increases. Figure 9b shows different surface morphologies and the increase in contact angle of the water droplets on different surface structures. The water contact angle measurement shows that the femtosecond laser treatment of Au turns its originally hydrophilic surface ($\theta_M \sim 74^\circ$) into a hydrophobic surface ($\theta_M \sim 108^\circ$). The θ_M measurements indicate that as the surface nano/microstructures increase, the θ_M significantly increases as well. Numerous studies [32,35,86–89] have shown that bioinspired surfaces with superwettability can be prepared using ultrashort pulse lasers. Alexandre Cunha et al. [90] generated hydrophilic surface textures on the surface of Ti-6Al-4V alloys by femtosecond laser processing. They show that the surface treatment of metal surfaces with femtosecond lasers is an effective technique for improving surface wettability. A. Y. Vorobyev et al. [91] prepared superhydrophobic and self-cleaning multifunctional surfaces using femtosecond laser pulses. Research by Erin Liu et al. [92] demonstrates that femtosecond fiber lasers can form layered structures on metal surfaces, demonstrating superhydrophobic, self-cleaning, and light-trapping properties. Sohail A. Jalil et al. [93] investigated the surface structure of femtosecond laser-induced gold (Au) and its effect on hydrophobicity. The result shows that the femtosecond laser processing turns originally hydrophilic Au into a superhydrophobic surface. It can be seen that surfaces with superwettability have a significant impact on other fields, such as for sensors, thermal management, biomedicine, etc. The long-term stability of LIPSSs' surface wetting properties (e.g., hydrophobicity or hydrophilicity) in applications will be a popular topic in the future.

A



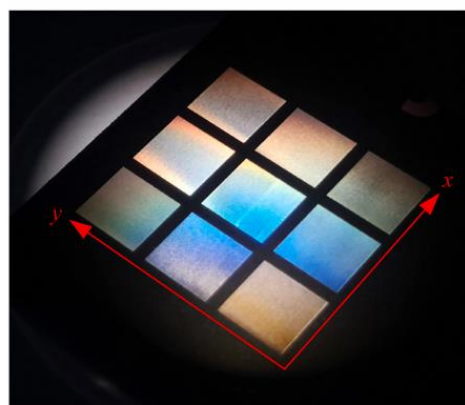
B



(a)

P	4.04 W	4.46 W	4.92 W
f	700 kHz	700 kHz	700 kHz
r	76.6%	76.6%	76.6%
	4.46 W	4.46 W	4.46 W
f	600 kHz	700 kHz	800 kHz
r	76.6%	76.6%	76.6%
	4.46 W	4.46 W	4.46 W
r	700 kHz	700 kHz	700 kHz
	88.3%	76.6%	53.3%

(b)



(c)



(d)

Figure 8. (A) Ref. [79] A portrait of Vincent van Gogh on stainless steel surfaces. (B) Ref. [80] (a) Optical images of the sample after laser irradiation, and (b) the corresponding laser parameters (P , Laser power; f , Laser repetition frequency; r , Pulse overlap rate between two adjacent scanning lines). (c) shows the optical images “nine-squares” captured in the dark environment, and (d) shows the color change in “JLU” when changing the shooting angle.

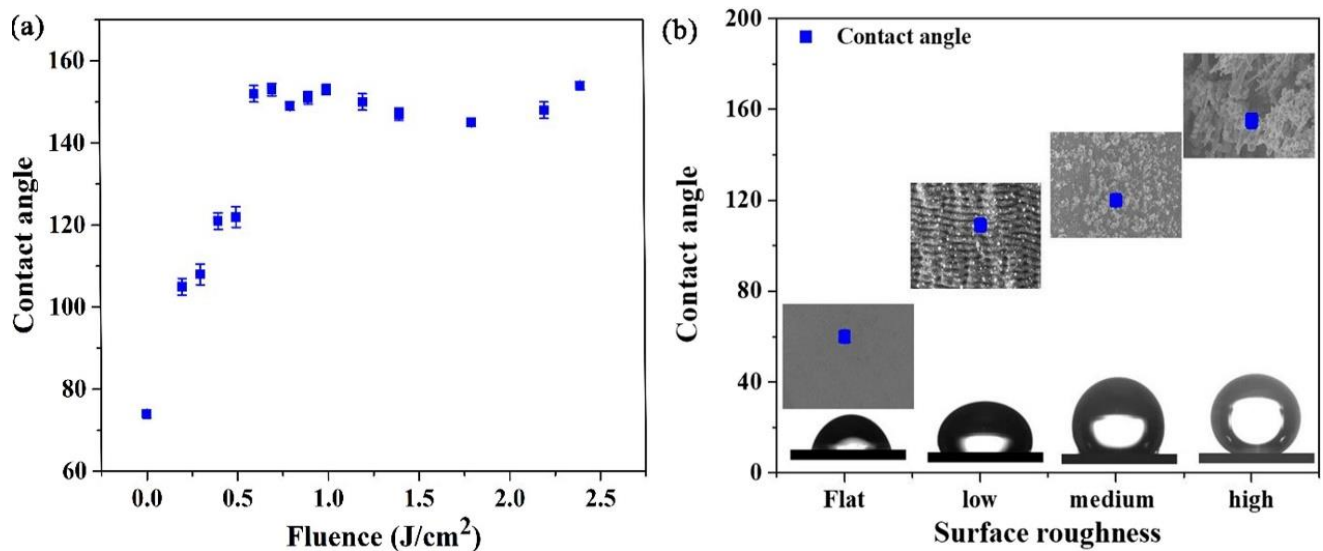


Figure 9. Ref. [93] (a) The measured contact angle values as a function of laser fluence. (b) The contact angle values measured on the initial surface roughness at low fluence. Corresponding surface morphologies are depicted in the insets.

4.3. Biomedical Applications

Another promising application area for LIPSS is biomedicine, which can inhibit the formation of bacterial biofilm and affect cell growth. Laser texturing has been used in the biomedical field as a method of altering surface morphology to potentially improve osseointegration [94–97]. Research [98–101] has shown that different surface topographies have a great influence on cell growth. Kai Borchering et al. [102] described the adhesion and shape of osteoblast-like cells (MG-63) after laser treatment of titanium alloys. Compared to pure titanium, the cell viability was improved on the structured surface, indicating good cytocompatibility. Alexandre Cunha et al. [94] prepared three types of surface textures by femtosecond laser: LIPSSs, nanopillars, and microcolumns covered with LIPSSs. Compared with the polished reference group, the cell area and adhesion area of human mesenchymal stem cells on the surface of the laser-treated titanium alloy are reduced. Xiao Luo et al. [103] applied femtosecond laser irradiation to produce three types of nano-ripples on the surface of pure titanium, and to investigate their anti-bacterial behavior and their biocompatibility. The three types of nano-ripples include LIPSSs (type 1 textures), nano-ripples interrupted by grooves (type 2 textures), and columns with overlapping LIPSS (type 3 textures). The control group is the mechanical polishing group. The results shows that three types of nano-ripples can prevent bacterial colonization and biofilm formation. As demonstrated in Figure 10a, the staining of F-actin and the nucleus shows the adhesion states of rat mesenchymal stem cells on the substrate surfaces. The red fluorescence is from Rhodamine cyclopeptide-stained F-actin. The blue fluorescence is from the DAPI-stained cell nucleus. The arrow indicates the direction of cell diffusion. As can be seen from Figure 10b, the spread of cells is oriented. Compared to the polished titanium, the spreading areas of laser-fabricated samples are significantly larger, which means the adhesion sites offered by the three types of nano-ripples are beneficial to cell attachment. Ning Liu et al. [54] uses femtosecond laser surface modification to establish a nano-ripple structure on the Fe-30Mn alloy surface. Compared to the polished sample, the nano-ripple structure surface exhibited a significant improvement in the biodegradation rate. Cell growth depends on the size of the surface topography of the material, so controlling the size of the surface morphology may be a key factor in controlling cell function. By using femtosecond lasers for surface modification, different surface properties can be prepared on the implant. Using a femtosecond laser to fabricate nano-ripples and grooves on the surface of materials is a promising way to improve the performance of the implant material.

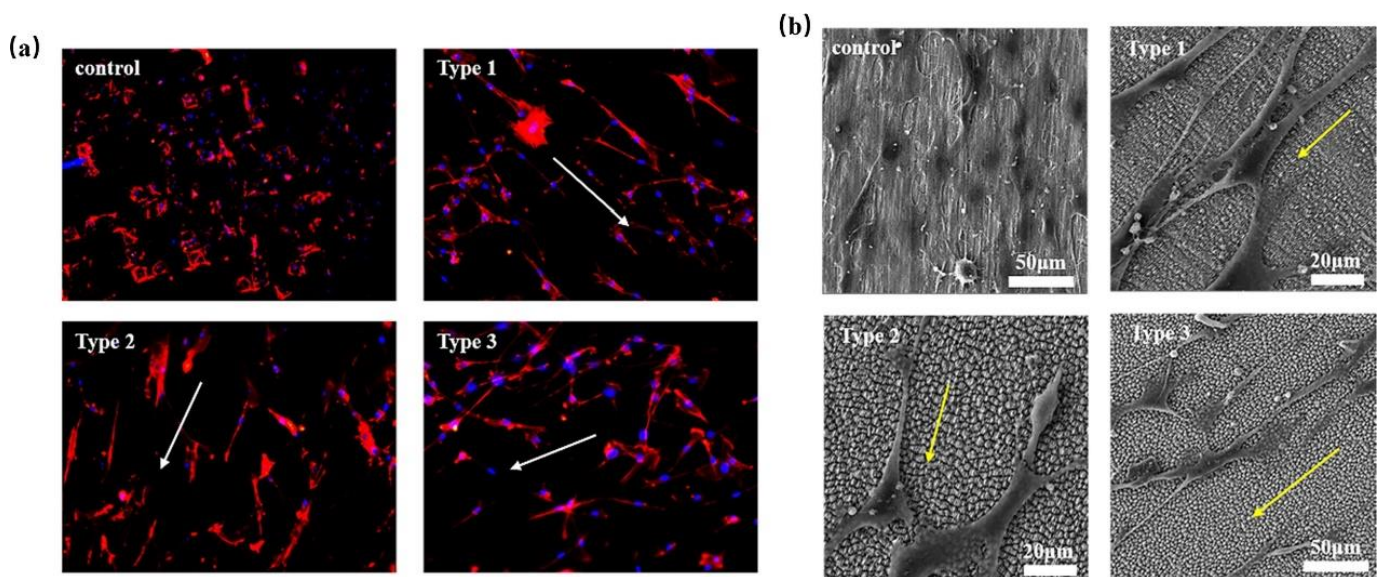


Figure 10. Ref. [103] Mesenchymal stem cells' adhesion on the polished surfaces and three types of nano-ripples after 72 h of incubations. (a) Fluorescence images of cytoskeletons; (b) SEM images of MSCs' adhesion states for the three types of nano-ripples. The both arrow indicates the direction of cell diffusion.

4.4. Reduction in Friction and Wear

LIPSS can exhibit beneficial tribological properties by reducing frictional wear. Surface topography and roughness have a significant impact on friction and wear [104]. Numerous studies [105–108] have shown that laser processing to prepare specific surface textures is an effective technique to improve surface friction performance. Jörn Bonse et al. [109] presented the latest advances in femtosecond laser surface texturing, observing the tribological properties of steel and the titanium alloy surface morphology (ripples, grooves, and spikes). Compared to the wear tracks on the surface of the polished sample, the wear tracks in the femtosecond laser processing area are almost invisible. The reason for its significant abrasion resistance is the LIPSS generated during the laser surface treatment. Figure 11 shows a sketch of the reciprocating sliding tribological test geometry (Figure 11a) along with top-view optical micrographs of the generated wear tracks on the polished Ti6Al4V alloy surface (Figure 11b) and the Spike-covered surface (Figure 11c). Additionally, top-view SEM micrographs revealing details from the wear tracks are presented (Figure 11d: initially polished, Figure 11e: LSFL, Figure 11f: Grooves, Figure 11g: Spikes). It is evident that on all laser-generated morphologies, the topmost regions have been partly worn, but the structures were not removed. The wear track and surface damage left on the polished surface is much larger than that in the laser-processed regions. The research of C. Florian et al. [110] demonstrated that femtosecond laser ablation forms a nanoscale morphology on the metal surface, resulting in a significant reduction in its coefficient of friction. Femtosecond laser treatments of metal surfaces inhibit adhesion tendencies by reducing the contact area, and the improvement in the tribological properties is due to the combined effect of LIPSSs.

4.5. Other Applications

Several other technical applications of LIPSS have been explored. Laser processing ablation obtains the desired surface features on the metal; such modified surfaces can be both beneficial and durable in phase-change heat transfer applications. Surface modification by ultra-short pulse lasers alters the heat transfer performances of the boiling system [111]. Since the LIPSSs can significantly increase the absorption rate of the surface, they will simultaneously lead to an increase in thermal radiation. Another potential application of LIPSS is related to catalytic activity in electrochemical processes [4], in which the active sur-

face area of the electrode material is critical to the efficiency of the electrochemical reaction. LIPSSs can be applied to energy-saving components and sensors [5]. Another application of LIPSSs is in chemical analyses based on surface-enhanced Raman spectroscopy. In the future, many will explore the established and new surface functions that be created through LIPSSs, so that these materials can be better applied in mechanical engineering, healthcare, aerospace, energy, and other fields.

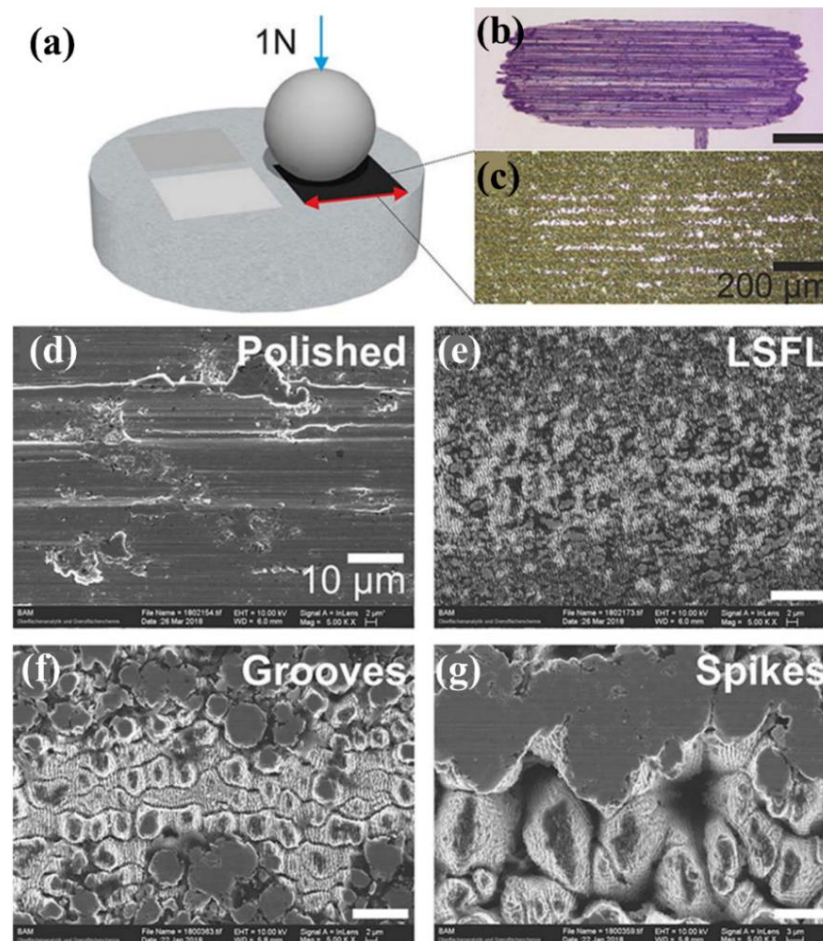


Figure 11. Ref. [110] Tribological performance of the samples after irradiation. (a) Sketch of the tribology setup using a steel ball of 100 Cr6 on the surface of the Ti6Al4V alloy sample. The final wear track achieved after 1000 sliding cycles is shown in (b) for the free surface and in (c) for a Spike-covered area as optical micrographs. SEM micrographs of the wear track on the different areas are shown in (d) for the initially polished surface, (e) LSFL, (f) Grooves, and (g) Spikes.

In summary, various patterns can be prepared by femtosecond lasers to improve the performance of materials. Due to the versatility of the femtosecond laser process, the correlation between surface morphology and alloy properties still has great research potential.

5. Summary and Outlook

The femtosecond laser is applied to biomedical materials as a surface modification technology. The laser-induced periodic structure generated by fs-laser action can improve the wear resistance, corrosion resistance, wetting, and biocompatibility of material surfaces. Although there have been many relevant reports, the mechanism of action of laser ablation materials to form special structures on the surface is still being explored. The correlation between surface patterns and material properties still needs to be studied continuously. In the future, numerical simulations will predictively simulate the laser processing parameters of the desired surface topography with the help of machine learning algorithms. The

relevant control parameters of functionalized surfaces are identified for better industrial applications. Another trend will be continuing to explore the creation of LIPSSs and their surface capabilities so that they can be better applied in mechanical engineering, healthcare, aerospace, information, and other fields.

Author Contributions: J.L. carried out the conception of the idea of the manuscript. H.S. and M.L. collected and collated the data. H.S. wrote the original draft. J.L. reviewed and revised the original draft. F.L. and D.Y. provided guidance for the revision of the manuscript. All authors have read and agreed to the published version of the manuscript.

Funding: This research received no external funding.

Institutional Review Board Statement: Not applicable.

Informed Consent Statement: Not applicable.

Data Availability Statement: The data supporting the finding of this study are available within the article.

Conflicts of Interest: The authors declare no conflict of interest.

References

1. Townes, C.H.; Chu, S. How the Laser Happened: Adventures of a Scientist. *Phys. Today* **1999**, *52*, 59–60. [[CrossRef](#)]
2. De Spence, K.P.; Sibbett, W. 60-Fsec Pulse Generation from a Self-Mode-Locked Ti:Sapphire Laser. *Opt. Lett.* **1991**, *16*, 42–44. [[CrossRef](#)] [[PubMed](#)]
3. Ali, B.; Litvinyuk, I.V.; Rybachuk, M. Femtosecond Laser Micromachining of Diamond: Current Research Status, Applications and Challenges. *Carbon* **2021**, *179*, 209–226. [[CrossRef](#)]
4. Wang, Y.; Zhao, Y.; Qu, L. Laser Fabrication of Functional Micro-Supercapacitors. *J. Energy Chem.* **2021**, *59*, 642–665. [[CrossRef](#)]
5. Chen, M.-Q.; He, T.-Y.; Zhao, Y. Review of Femtosecond Laser Machining Technologies for Optical Fiber Microstructures Fabrication. *Opt. Laser Technol.* **2022**, *147*, 107628. [[CrossRef](#)]
6. Zhao, J.; Zhao, Y.; Peng, Y.; Lv, R.-Q.; Zhao, Q. Review of Femtosecond Laser Direct Writing Fiber-Optic Structures Based on Refractive index Modification and Their Applications. *Opt. Laser Technol.* **2022**, *146*, 107473. [[CrossRef](#)]
7. Kumar, R.; del Pino, A.P.; Sahoo, S.; Singh, R.K.; Tan, W.K.; Kar, K.K.; Matsuda, A.; Joanni, E. Laser Processing of Graphene and Related Materials for Energy Storage: State of the Art and Future Prospects. *Prog. Energy Combust. Sci.* **2022**, *91*, 100981. [[CrossRef](#)]
8. Siuzdak, K.; Haryński, Ł.; Wawrzyniak, J.; Grochowska, K. Review on Robust Laser Light Interaction with Titania—Patterning, Crystallisation and Ablation Processes. *Prog. Solid State Chem.* **2021**, *62*, 100297. [[CrossRef](#)]
9. Zhao, B.; Zheng, X.; Lei, Y.; Xie, H.; Zou, T.; Yuan, G.; Xin, W.; Yang, J. High-Efficiency-and-Quality Nanostructuring of Molybdenum Surfaces by Orthogonally Polarized Blue Femtosecond Lasers. *Appl. Surf. Sci.* **2022**, *572*, 151371. [[CrossRef](#)]
10. Nivas, J.J.; Allahyari, E.; Skoulas, E.; Bruzzese, R.; Fittipaldi, R.; Tsididis, G.D.; Stratakis, E.; Amoroso, S. Incident Angle Influence on Ripples and Grooves Produced by Femtosecond Laser Irradiation of Silicon. *Appl. Surf. Sci.* **2021**, *570*, 151150. [[CrossRef](#)]
11. Museur, L.; Manousaki, A.; Anglos, D.; Tsididis, G.; Kanaev, A. Pathways control in modification of solid surfaces induced by temporarily separated femtosecond laser pulses. *Appl. Surf. Sci.* **2021**, *566*, 150611. [[CrossRef](#)]
12. Dashtbozorg, B.; Penchev, P.; Romano, J.-M.; Li, X.; Sammons, R.L.; Dimov, S.; Dong, H. Development of surfaces with antibacterial durability through combined phase plasma hardening and athermal femtosecond laser texturing. *Appl. Surf. Sci.* **2021**, *565*, 150594. [[CrossRef](#)]
13. Kotsiuba, Y.; Hevko, I.; Bellucci, S.; Gnilytskyi, I. Bitmap and vectorial hologram recording by using femtosecond laser pulses. *Sci. Rep.* **2021**, *11*, 16406. [[CrossRef](#)] [[PubMed](#)]
14. Zhang, T.; Wei, D.; Lu, E.; Wang, W.; Wang, K.; Li, X.; Zhang, L.-C.; Kato, H.; Lu, W.; Wang, L. Microstructure evolution and deformation mechanism of A+B dual-phase Ti-Xnb-Yta-2Zr alloys with high performance. *J. Mater. Sci. Technol.* **2022**, *131*, 68–81. [[CrossRef](#)]
15. Guo, L.; Naghavi, S.A.; Wang, Z.; Varma, S.N.; Han, Z.; Yao, Z.; Wang, L.; Liu, C. On the design evolution of hip implants: A review. *Mater. Des.* **2022**, *216*, 110552. [[CrossRef](#)]
16. Wang, J.C.; Liu, Y.J.; Liang, S.X.; Zhang, Y.S.; Wang, L.Q.; Sercombe, T.B.; Zhang, L.C. Comparison of microstructure and mechanical behavior of Ti-35Nb manufactured by laser powder bed fusion from elemental powder mixture and prealloyed powder. *J. Mater. Sci. Technol.* **2022**, *105*, 1–16. [[CrossRef](#)]
17. Cui, Y.-W.; Chen, L.-Y.; Qin, P.; Li, R.; Zang, Q.; Peng, J.; Zhang, L.; Lu, S.; Wang, L.; Zhang, L.-C. Metastable pitting corrosion behavior of laser powder bed fusion produced Ti-6Al-4V in Hank's solution. *Corros. Sci.* **2022**, *203*, 110333. [[CrossRef](#)]
18. Candel, J.J.; Amigó, V. Recent advances in laser surface treatment of titanium alloys. *J. Laser Appl.* **2011**, *23*, 022005. [[CrossRef](#)]
19. Mohazzab, B.F.; Jaleh, B.; Fattah-alhosseini, A.; Mahmoudi, F.; Momeni, A. Laser surface treatment of pure titanium: Microstructural analysis, wear properties, and corrosion behavior of titanium carbide coatings in Hank's physiological solution. *Surf. Interfaces* **2020**, *20*, 100597. [[CrossRef](#)]

20. Liu, R.; Chi, Z.; Cao, L.; Weng, Z.; Wang, L.; Li, L.; Saeed, S.; Lian, Z.; Wang, Z. Fabrication of biomimetic superhydrophobic and anti-icing Ti6al4v alloy surfaces by direct laser interference lithography and hydrothermal treatment. *Appl. Surf. Sci.* **2020**, *534*, 147576. [[CrossRef](#)]
21. Wang, L.; Xie, L.; Shen, P.; Fan, Q.; Wang, W.; Wang, K.; Lu, W.; Hua, L.; Zhang, L.-C. Surface microstructure and mechanical properties of Ti-6al-4v/Ag nanocomposite prepared by fsp. *Mater. Charact.* **2019**, *153*, 175–183. [[CrossRef](#)]
22. Wang, L.; Xie, L.; Lv, Y.; Zhang, L.-C.; Chen, L.-Y.; Meng, Q.; Qu, J.; Zhang, D.; Lu, W. Microstructure evolution and superelastic behavior in Ti-35nb-2ta-3zr alloy processed by friction stir processing. *Acta Mater.* **2017**, *131*, 499–510. [[CrossRef](#)]
23. Thesleff, A.; Ortiz-Catalan, M.; Branemark, R. Low plasticity burnishing improves fretting fatigue resistance in bone-anchored implants for amputation prostheses. *Med. Eng. Phys.* **2022**, *100*, 103755. [[CrossRef](#)]
24. Li, Z.-X.; Bao, Y.-T.; Wu, L.-K.; Cao, F.-H. Oxidation and tribological properties of anodized Ti45al8.5nb alloy. *Trans. Nonferrous Met. Soc. China* **2021**, *31*, 3439–3451. [[CrossRef](#)]
25. Kazemi, M.; Ahangarani, S.; Esmailian, M.; Shanaghi, A. Investigating the corrosion performance of Ti-6al-4v biomaterial alloy with hydroxyapatite coating by artificial neural network. *Mater. Sci. Eng.* **2022**, *278*, 115644. [[CrossRef](#)]
26. Garrido, B.; Dosta, S.; Cano, I.G. Bioactive glass coatings obtained by thermal spray: Current status and future challenges. *Boletín De La Soc. Española De Cerámica Y Vidr.* **2021**, *in press*. [[CrossRef](#)]
27. Gabor, R.; Cvrček, L.; Doubková, M.; Nehasil, V.; Hlinka, J.; Unucka, P.; Buřil, M.; Podepřelová, A.; Seidlerová, J.; Bačáková, L. Hybrid coatings for orthopaedic implants formed by physical vapour deposition and microarc oxidation. *Mater. Des.* **2022**, *219*, 110811. [[CrossRef](#)]
28. Yang, Z.; Zhu, C.; Zheng, N.; Le, D.; Zhou, J. Superhydrophobic surface preparation and wettability transition of titanium alloy with micro/nano hierarchical texture. *Materials* **2018**, *11*, 2210. [[CrossRef](#)]
29. Gräf, S. Formation of laser-induced periodic surface structures on different materials: Fundamentals, properties and applications. *Adv. Opt. Technol.* **2020**, *9*, 11–39. [[CrossRef](#)]
30. Liang, C.; Hu, Y.; Wang, H.; Xia, D.; Li, Q.; Zhang, J.; Yang, J.; Li, B.; Li, H.; Han, D.; et al. Biomimetic cardiovascular stents for in vivo re-endothelialization. *Biomaterials* **2016**, *103*, 170–182. [[CrossRef](#)]
31. Khorkov, K.S.; Kochuev, D.A.; Dzus, M.A.; Prokoshev, V.G. Wettability surface control on stainless steel by lipss formation. *J. Phys. Conf. Ser.* **2021**, *1822*, 012010. [[CrossRef](#)]
32. Ijaola, A.O.; Bamidele, E.A.; Akisin, C.J.; Bello, I.T.; Oyatobo, A.T.; Abdulkareem, A.; Farayibi, P.K.; Asmatulu, E. Wettability transition for laser textured surfaces: A comprehensive review. *Surf. Interfaces* **2020**, *21*, 100802. [[CrossRef](#)]
33. Boltaev, G.S.; Alghabra, M.S.; Iqbal, M.; Ganeev, R.A.; Alnaser, A.S. Creation of azimuthally and radially directed laser-induced periodic structures on large tantalum surface. *J. Phys. Appl. Phys.* **2021**, *54*, 185109. [[CrossRef](#)]
34. Zhang, Y.; Cheng, K.; Cao, K.; Jiang, Q.; Chen, T.; Zhang, S.; Feng, D.; Sun, Z.; Jia, T. Periodic subwavelength ripples on a si surface induced by a single temporally shaped femtosecond laser pulse: Enhanced periodic energy deposition and reduced residual thermal effect. *J. Phys. Appl. Phys.* **2021**, *54*, 385106. [[CrossRef](#)]
35. Yang, C.-J.; Mei, X.-S.; Tian, Y.-L.; Zhang, D.-W.; Li, Y.; Liu, X.-P. Modification of wettability property of titanium by laser texturing. *Int. J. Adv. Manuf. Technol.* **2016**, *87*, 1663–1670. [[CrossRef](#)]
36. Yang, L.; Wei, J.; Ma, Z.; Song, P.; Ma, J.; Zhao, Y.; Huang, Z.; Zhang, M.; Yang, F.; Wang, X. The Fabrication of micro/nano structures by laser machining. *Nanomaterials* **2019**, *9*, 1789. [[CrossRef](#)]
37. Bonse, J.; Hohm, S.; Kirner, S.V.; Rosenfeld, A.; Kruger, J. Laser-induced periodic surface structures—A scientific evergreen. *IEEE J. Sel. Top. Quantum Electron.* **2017**, *23*, 1–15. [[CrossRef](#)]
38. Bonse, J.; Gräf, S. Maxwell meets marangoni—A review of theories on laser-induced periodic surface structures. *Laser Photonics Rev.* **2020**, *14*, 2000215. [[CrossRef](#)]
39. Bonse, J. Quo vadis lipss? Recent and future trends on laser-induced periodic surface structures. *Nanomaterials* **2020**, *10*, 1950. [[CrossRef](#)]
40. Kirner, S.V.; Wirth, T.; Sturm, H.; Krüger, J.; Bonse, J. Nanometer-resolved chemical analyses of femtosecond laser-induced periodic surface structures on titanium. *J. Appl. Phys.* **2017**, *122*, 104901. [[CrossRef](#)]
41. Bonse, J.; Munz, M.; Sturm, H. Structure Formation on the surface of indium phosphide irradiated by femtosecond laser pulses. *J. Appl. Phys.* **2005**, *97*, 013538. [[CrossRef](#)]
42. Varlamova, O. Evolution of femtosecond laser induced surface structures at low number of pulses near the ablation threshold. *J. Laser Micro/Nanoeng.* **2013**, *8*, 300–303. [[CrossRef](#)]
43. Reif, J.; Varlamova, O.; Uhlig, S.; Varlamov, S.; Bestehorn, M. On the physics of self-organized nanostructure formation upon femtosecond laser ablation. *Appl. Phys.* **2014**, *117*, 179–184. [[CrossRef](#)]
44. Liu, R.; Zhang, D.; Li, Z. Femtosecond laser induced simultaneous functional nanomaterial synthesis, in situ deposition and hierarchical lipss nanostructuring for tunable antireflectance and iridescence applications. *J. Mater. Sci. Technol.* **2021**, *89*, 179–185. [[CrossRef](#)]
45. Razi, S.; Varlamova, O.; Reif, J.; Bestehorn, M.; Varlamov, S.; Mollabashi, M.; Madanipour, K.; Ratzke, M. Birth of periodic micro/nano structures on 316l stainless steel surface following femtosecond laser irradiation; single and multi scanning study. *Opt. Laser Technol.* **2018**, *104*, 8–16. [[CrossRef](#)]
46. Zagoranskiy, I.; Lorenz, P.; Ehrhardt, M.; Zimmer, K. Guided self-organization of nanodroplets induced by nanosecond ir laser radiation of molybdenum films on sapphire. *Opt. Lasers Eng.* **2019**, *113*, 55–61. [[CrossRef](#)]

47. Bronnikov, K.; Gladkikh, S.; Okotrub, K.; Simanchuk, A.; Zhizhchenko, A.; Kuchmizhak, A.; Dostovalov, A. Regulating morphology and composition of laser-induced periodic structures on titanium films with femtosecond laser wavelength and ambient environment. *Nanomaterials* **2022**, *12*, 306. [[CrossRef](#)]
48. Zhang, H.; Colombier, J.-P.; Witte, S. Laser-induced periodic surface structures: Arbitrary angles of incidence and polarization states. *Phys. Rev.* **2020**, *101*, 245430. [[CrossRef](#)]
49. Echlin, M.P.; Titus, M.S.; Straw, M.; Gumbsch, P.; Pollock, T.M. Materials Response to glancing incidence femtosecond laser ablation. *Acta Mater.* **2017**, *124*, 37–46. [[CrossRef](#)]
50. Schnell, G.; Lund, H.; Bartling, S.; Polley, C.; Riaz, A.; Senz, V.; Springer, A.; Seitz, H. Heat Accumulation during femtosecond laser treatment at high repetition rate—A morphological, chemical and crystallographic characterization of self-organized structures on Ti6Al4V. *Appl. Surf. Sci.* **2021**, *570*, 151115. [[CrossRef](#)]
51. Dou, H.-Q.; Liu, H.; Xu, S.; Chen, Y.; Miao, X.; Lü, H.; Jiang, X. Influence of laser fluences and scan speeds on the morphologies and wetting properties of titanium alloy. *Optik* **2020**, *224*, 165443. [[CrossRef](#)]
52. Wang, R.; Dong, X.; Wang, K.; Sun, X.; Fan, Z.; Duan, W.; Jun, M.B.-G. Polarization effect on hole evolution and periodic microstructures in femtosecond laser drilling of thermal barrier coated superalloys. *Appl. Surf. Sci.* **2021**, *537*, 148001. [[CrossRef](#)]
53. Gazizova, M.Y.; Smirnov, N.A.; Kudrayshov, S.I.; Shugurov, V.V. The effect of femtosecond laser treatment on the tribological properties of titanium nitride. *Iop Conf. Ser. Mater. Sci. Eng.* **2020**, *862*, 022054. [[CrossRef](#)]
54. Liu, N.; Sun, Y.; Wang, H.; Liang, C. Femtosecond laser-induced nanostructures on Fe-30 mn surfaces for biomedical applications. *Opt. Laser Technol.* **2021**, *139*, 106986. [[CrossRef](#)]
55. Bonse, J.; Krüger, J.; Höhm, S.; Rosenfeld, A. Femtosecond laser-induced periodic surface structures. *J. Laser Appl.* **2012**, *24*, 042006. [[CrossRef](#)]
56. Xu, S.-Z.; Dou, H.-Q.; Sun, K.; Ye, Y.-Y.; Li, Z.; Wang, H.-J.; Liao, W.; Liu, H.; Miao, X.-X.; Yuan, X.-D.; et al. Scan speed and fluence effects in femtosecond laser induced micro/nano-structures on the surface of fused silica. *J. Non-Cryst. Solids* **2018**, *492*, 56–62. [[CrossRef](#)]
57. Skoulas, E.; Manousaki, A.; Fotakis, C.; Stratakis, E. Biomimetic surface structuring using cylindrical vector femtosecond laser beams. *Sci. Rep.* **2017**, *7*, srep45114. [[CrossRef](#)] [[PubMed](#)]
58. Ji, X.; Jiang, L.; Li, X.; Han, W.; Liu, Y.; Wang, A.; Lu, Y. Femtosecond laser-induced cross-periodic structures on a crystalline silicon surface under low pulse number irradiation. *Appl. Surf. Sci.* **2015**, *326*, 216–221. [[CrossRef](#)]
59. Li, R.; Zhou, W.; Zhou, C.; Qi, Q.; Li, Y.; Yang, Y.; Zhang, W.; Zhang, P.; Dai, S.; Xu, T. Laser damage threshold of Ge8as23s69 films irradiated under single—And multiple-pulse femtosecond laser. *Ceram. Int.* **2022**, *48*, 8341–8348. [[CrossRef](#)]
60. Fraggelakis, F.; Stratakis, E.; Loukakos, P.A. Control of periodic surface structures on silicon by combined temporal and polarization shaping of femtosecond laser pulses. *Appl. Surf. Sci.* **2018**, *444*, 154–160. [[CrossRef](#)]
61. Han, W.; Han, Z.; Yuan, Y.; Wang, S.; Li, X.; Liu, F. Continuous control of microlens morphology on Si based on the polarization-dependent femtosecond laser induced periodic surface structures modulation. *Opt. Laser Technol.* **2019**, *119*, 105629. [[CrossRef](#)]
62. Fraggelakis, F.; Mincuzzi, G.; Lopez, J.; Manek-Hönninger, I.; Kling, R. Controlling 2d Laser nano structuring over large area with double femtosecond pulses. *Appl. Surf. Sci.* **2019**, *470*, 677–686. [[CrossRef](#)]
63. Romano, J.-M.; Garcia-Giron, A.; Penchev, P.; Dimov, S. Triangular laser-induced submicron textures for functionalising stainless steel surfaces. *Appl. Surf. Sci.* **2018**, *440*, 162–169. [[CrossRef](#)]
64. Milles, S.; Voisiat, B.; Nitschke, M.; Lasagni, A.F. Influence of roughness achieved by periodic structures on the wettability of aluminum using direct laser writing and direct laser interference patterning technology. *J. Mater. Process. Technol.* **2019**, *270*, 142–151. [[CrossRef](#)]
65. Vanithakumari, S.C.; Kumar, C.A.; Thinaharan, C.; Kishor, G.R.; George, R.P.; Kaul, R.; Bindra, K.S.; John, P. Laser patterned titanium surfaces with superior antibiofouling, superhydrophobicity, self-cleaning and durability: Role of line spacing. *Surf. Coat. Technol.* **2021**, *418*, 127257.
66. Durbach, S.; Hampp, N. Generation of 2d-arrays of anisotropically shaped nanoparticles by nanosecond laser-induced periodic surface patterning. *Appl. Surf. Sci.* **2021**, *556*, 149803. [[CrossRef](#)]
67. Mangababu, A.; Goud, R.S.P.; Byram, C.; Rathod, J.; Banerjee, D.; Soma, V.R.; Rao, S.N. Multi-functional gallium arsenide nanoparticles and nanostructures fabricated using picosecond laser ablation. *Appl. Surf. Sci.* **2022**, *589*, 152802. [[CrossRef](#)]
68. Yao, C.; Ye, Y.; Jia, B.; Li, Y.; Ding, R.; Jiang, Y.; Wang, Y.; Yuan, X. Polarization and fluence effects in femtosecond laser induced micro/nano structures on stainless steel with antireflection property. *Appl. Surf. Sci.* **2017**, *425*, 1118–1124. [[CrossRef](#)]
69. Sun, Y.; Chen, L.; Liu, N.; Wang, H.; Liang, C. Laser-modified Fe–30 mn Surfaces with promoted biodegradability and biocompatibility toward biological applications. *J. Mater. Sci.* **2021**, *56*, 13772–13784. [[CrossRef](#)]
70. Shin, S.; Hur, J.-G.; Park, J.K.; Kim, D.-H. Thermal damage free material processing using femtosecond laser pulses for fabricating fine metal masks: Influences of laser fluence and pulse repetition rate on processing quality. *Opt. Laser Technol.* **2021**, *134*, 106618. [[CrossRef](#)]
71. Xin, Z.; Ren, N.; Ren, Y.; Yue, X.; Han, Q.; Zhou, W.; Tao, Y.; Ye, Y. In-situ nitriding on the textured titanium alloy using femtosecond laser. *J. Mater. Res. Technol.* **2022**, *19*, 466–471. [[CrossRef](#)]
72. Yalishiev, V.; Iqbal, M.; Kim, V.; Alnaser, A.S. Effect of processing environment on the wettability behavior of laser-processed titanium. *J. Phys. Appl. Phys.* **2021**, *55*, 045401. [[CrossRef](#)]

73. Yang, Y.Y.J.; Liang, C.; Wang, H.; Zhu, X.; Zhang, N. Surface microstructuring of Ti plates by femtosecond lasers in liquid ambiances: A new approach to improving biocompatibility. *Opt. Express* **2009**, *9*, 21124–21133. [[CrossRef](#)] [[PubMed](#)]
74. Dong, J.; Pacella, M.; Liu, Y.; Zhao, L. Surface engineering and the application of laser-based processes to stents—A review of the latest development. *Bioact. Mater.* **2022**, *10*, 159–184. [[CrossRef](#)] [[PubMed](#)]
75. Stratakis, E.; Bonse, J.; Heitz, J.; Siegel, J.; Tsibidis, G.D.; Skoulas, E.; Papadopoulos, A.; Mimidis, A.; Joel, A.C.; Comanns, P.; et al. Laser engineering of biomimetic surfaces. *Mater. Sci. Eng. Rep.* **2020**, *141*, 100562. [[CrossRef](#)]
76. Wang, L.; Yin, K.; Zhu, Z.; Deng, Q.; Huang, Q. Femtosecond Laser engraving micro/nanostructured poly (ether-ether-ketone) surface with superhydrophobic and photothermal ability. *Surf. Interfaces* **2022**, *31*, 102013. [[CrossRef](#)]
77. Liu, K.; Yang, C.; Zhang, S.; Wang, Y.; Zou, R.; Alamusi; Deng, Q.; Hu, N. Laser direct writing of a multifunctional superhydrophobic composite strain sensor with excellent corrosion resistance and anti-icing/deicing performance. *Mater. Des.* **2022**, *218*, 110689. [[CrossRef](#)]
78. Yin, K.; Du, H.; Luo, Z.; Dong, X.; Duan, J.-A. Multifunctional micro/nano-patterned ptfе near-superamphiphobic surfaces achieved by a femtosecond laser. *Surf. Coat. Technol.* **2018**, *345*, 53–60. [[CrossRef](#)]
79. Dusser, B.S.Z.; Soder, H.; Faure, N.; Colombier, J.; Jourlin, M.; Audouard, E. Controlled nanostructures formation by ultra fast laser pulses for color marking. *Opt. Express* **2010**, *18*, 2913–2924. [[CrossRef](#)]
80. Wang, C.; Huang, H.; Qian, Y.; Zhang, Z.; Huang, W.; Yan, J. Nitrogen assisted formation of large-area ripples on Ti6al4v surface by nanosecond pulse laser irradiation. *Precis. Eng.* **2022**, *73*, 244–256. [[CrossRef](#)]
81. Zhang, D.; Liu, R.; Li, Z. Irregular lipss produced on metals by single linearly polarized femtosecond laser. *Int. J. Extrem. Manuf.* **2021**, *4*, 015102. [[CrossRef](#)]
82. Milovanović, D.S.; Gaković, B.; Radu, C.; Zamfirescu, M.; Radak, B.; Petrović, S.; Miladinović, Z.R.; Mihailescu, I.N. Femtosecond laser surface patterning of steel and titanium alloy. *Phys. Scr.* **2014**, *T162*, 014017. [[CrossRef](#)]
83. Florian, C.; Kirner, S.V.; Krüger, J.; Bonse, J. Surface functionalization by laser-induced periodic surface structures. *J. Laser Appl.* **2020**, *32*, 022063. [[CrossRef](#)]
84. Stoian, R.; Colombier, J.-P. Advances in ultrafast laser structuring of materials at the nanoscale. *Nanophotonics* **2020**, *9*, 4665–4688. [[CrossRef](#)]
85. Gnilitzky, I.; Derrien, T.J.-Y.; Levy, Y.; Bulgakova, N.M.; Mocek, T.; Orazi, L. High-Speed manufacturing of highly regular femtosecond laser-induced periodic surface structures: Physical origin of regularity. *Sci. Rep.* **2017**, *7*, 8485. [[CrossRef](#)] [[PubMed](#)]
86. Wang, S.; Liu, K.; Yao, X.; Jiang, L. Bioinspired surfaces with superwettability: New insight on theory, design, and applications. *Chem. Rev.* **2015**, *115*, 8230–8293. [[CrossRef](#)]
87. Wang, Y.; Zhang, J.; Li, K.; Hu, J. Surface characterization and biocompatibility of isotropic microstructure prepared by uv laser. *J. Mater. Sci. Technol.* **2021**, *94*, 136–146. [[CrossRef](#)]
88. Simoes, I.G.; Dos Reis, A.C.; Da Costa Valente, M.L. Analysis of the influence of surface treatment by high-power laser irradiation on the surface properties of titanium dental implants: A systematic review. *J. Prosthet. Dent.* **2021**, *in press*. [[CrossRef](#)]
89. Yang, K.; Shi, J.; Wang, L.; Chen, Y.; Liang, C.; Yang, L.; Wang, L.-N. Bacterial anti-adhesion surface design: Surface patterning, roughness and wettability: A review. *J. Mater. Sci. Technol.* **2022**, *99*, 82–100. [[CrossRef](#)]
90. Cunha, A.; Serro, A.P.; Oliveira, V.; Almeida, A.; Vilar, R.; Durrieu, M.C. Wetting behaviour of femtosecond laser textured Ti-6al-4v surfaces. *Appl. Surf. Sci.* **2013**, *265*, 688–696. [[CrossRef](#)]
91. Vorobyev, A.Y.; Guo, C. Multifunctional surfaces produced by femtosecond laser pulses. *J. Appl. Phys.* **2015**, *117*, 033103. [[CrossRef](#)]
92. Liu, E.; Lee, H.J.; Lu, X. Superhydrophobic surfaces enabled by femtosecond fiber laser-written nanostructures. *Appl. Sci.* **2020**, *10*, 2678. [[CrossRef](#)]
93. Jalil, S.A.; Akram, M.; Bhat, J.A.; Hayes, J.J.; Singh, S.C.; ElKabbash, M.; Guo, C. Creating superhydrophobic and antibacterial surfaces on gold by femtosecond laser pulses. *Appl. Surf. Sci.* **2020**, *506*, 144952. [[CrossRef](#)] [[PubMed](#)]
94. Cunha, A.; Zouani, O.F.; Plawinski, L.; Botelho do Rego, A.M.; Almeida, A.; Vilar, R.; Durrieu, M.C. Human mesenchymal stem cell behavior on femtosecond laser-textured Ti-6al-4v surfaces. *Nanomedicine* **2015**, *10*, 725–739. [[CrossRef](#)] [[PubMed](#)]
95. Dumas, V.; Guignandon, A.; Vico, L.; Mauclair, C.; Zapata, X.; Linossier, M.T.; Bouleftour, W.; Granier, J.; Peyroche, S.; Dumas, J.-C.; et al. Femtosecond laser nano/micro patterning of titanium influences mesenchymal stem cell adhesion and commitment. *Biomed. Mater.* **2015**, *10*, 055002. [[CrossRef](#)] [[PubMed](#)]
96. Kumari, R.; Scharnweber, T.; Pflöging, W.; Besser, H.; Majumdar, J.D. Laser surface textured titanium alloy (Ti-6al-4v)—Part Ii—studies on bio-compatibility. *Appl. Surf. Sci.* **2015**, *357*, 750–758. [[CrossRef](#)]
97. Klos, A.; Sedao, X.; Itina, T.E.; Helfenstein-Didier, C.; Donnet, C.; Peyroche, S.; Vico, L.; Guignandon, A.; Dumas, V. Ultrafast laser processing of nanostructured patterns for the control of cell adhesion and migration on titanium alloy. *Nanomaterials* **2020**, *10*, 864. [[CrossRef](#)] [[PubMed](#)]
98. Raimbault, O.; Benayoun, S.; Anselme, K.; Mauclair, C.; Bourgade, T.; Kietzig, A.-M.; Girard-Lauriault, P.-L.; Valette, S.; Donnet, C. The effects of femtosecond laser-textured Ti-6al-4v on wettability and cell response. *Mater. Sci. Eng. Mater. Biol. Appl.* **2016**, *69*, 311–320. [[CrossRef](#)]
99. Wang, Y.; Yu, Z.; Li, K.; Hu, J. Study on the effect of surface characteristics of short-pulse laser patterned titanium alloy on cell proliferation and osteogenic differentiation. *Mater. Sci. Eng. Mater. Biol. Appl.* **2021**, *128*, 112349. [[CrossRef](#)]

100. Stanciuc, A.-M.; Flamant, Q.; Sprecher, C.M.; Alini, M.; Anglada, M.; Peroglio, M. Femtosecond laser multi-patterning of zirconia for screening of cell-surface interactions. *J. Eur. Ceram. Soc.* **2018**, *38*, 939–948. [[CrossRef](#)]
101. Kedia, S.; Bonagani, S.K.; Majumdar, A.G.; Kain, V.; Subramanian, M.; Maiti, N.; Nilaya, J.P. Nanosecond laser surface texturing of type 316L stainless steel for contact guidance of bone cells and superior corrosion resistance. *Colloid Interface Sci. Commun.* **2021**, *42*, 100419. [[CrossRef](#)]
102. Borchering, K.; Marx, D.; Gätjen, L.; Specht, U.; Salz, D.; Thiel, K.; Wildemann, B.; Grunwald, I. Impact of laser structuring on medical-grade titanium: Surface characterization and in vitro evaluation of osteoblast attachment. *Materials* **2020**, *13*, 2000. [[CrossRef](#)] [[PubMed](#)]
103. Luo, X.; Yao, S.; Zhang, H.; Cai, M.; Liu, W.; Pan, R.; Chen, C.; Wang, X.; Wang, L.; Zhong, M. Biocompatible nano-ripples structured surfaces induced by femtosecond laser to rebel bacterial colonization and biofilm formation. *Opt. Laser Technol.* **2020**, *124*, 105973. [[CrossRef](#)]
104. Luo, J.; Sun, W.; Duan, R.; Yang, W.; Chan, K.; Ren, F.; Yang, X.-S. Laser surface treatment-introduced gradient nanostructured titanium refractory high-entropy alloy with significantly enhanced wear resistance. *J. Mater. Sci. Technol.* **2022**, *110*, 43–56. [[CrossRef](#)]
105. Bonse, J.; Koter, R.; Hartelt, M.; Spaltmann, D.; Pentzien, S.; Höhm, S.; Rosenfeld, A.; Krüger, J. Tribological performance of femtosecond laser-induced periodic surface structures on titanium and a high toughness bearing steel. *Appl. Surf. Sci.* **2015**, *336*, 21–27. [[CrossRef](#)]
106. Bonse, J.; Koter, R.; Hartelt, M.; Spaltmann, D.; Pentzien, S.; Höhm, S.; Rosenfeld, A.; Krüger, J. Femtosecond laser-induced periodic surface structures on steel and titanium alloy for tribological applications. *Appl. Phys.* **2014**, *117*, 103–110. [[CrossRef](#)]
107. Bonse, J.; Höhm, S.; Koter, R.; Hartelt, M.; Spaltmann, D.; Pentzien, S.; Rosenfeld, A.; Krüger, J. Tribological performance of sub-100-Nm femtosecond laser-induced periodic surface structures on titanium. *Appl. Surf. Sci.* **2016**, *374*, 190–196. [[CrossRef](#)]
108. Pan, X.; He, W.; Cai, Z.; Wang, X.; Liu, P.; Luo, S.; Zhou, L. Investigations on femtosecond laser-induced surface modification and periodic micropatterning with anti-friction properties on Ti6Al4V titanium alloy. *Chin. J. Aeronaut.* **2022**, *35*, 521–537. [[CrossRef](#)]
109. Bonse, J.; Kirner, S.V.; Griepentrog, M.; Spaltmann, D.; Krüger, J. Femtosecond laser texturing of surfaces for tribological applications. *Materials* **2018**, *11*, 801. [[CrossRef](#)]
110. Florian, C.; Wonneberger, R.; Undisz, A.; Kirner, S.V.; Wasmuth, K.; Spaltmann, D.; Krüger, J.; Bonse, J. Chemical effects during the formation of various types of femtosecond laser-generated surface structures on titanium alloy. *Appl. Phys.* **2020**, *126*, 266. [[CrossRef](#)]
111. Kumar, G.U.; Suresh, S.; Kumar, C.S.; Back, S.; Kang, B.; Lee, H.J. A review on the role of laser textured surfaces on boiling heat transfer. *Appl. Therm. Eng.* **2020**, *174*, 115274. [[CrossRef](#)]